ARL-TR-10305 • MAR 2026

Additive Manufacturing of Gd-Doped CeO_2 Architectures via a Custom-Developed Printable Ceramic Resin for Ethanol Catalytic Partial Oxidation

by Gene Yang, Jiangtian Li, and Deryn Chu

NOTICES

Disclaimers

The findings in this report are not to be construed as an official Department of the Army position unless so designated by other authorized documents.

Citation of manufacturer's or trade names does not constitute an official endorsement or approval of the use thereof.

Destroy this report when it is no longer needed. Do not return it to the originator.

ARL-TR-10305 ● MAR 2026

Additive Manufacturing of Gd-Doped CeO_2 Architectures via a Custom-Developed Printable Ceramic Resin for Ethanol Catalytic Partial Oxidation

Gene Yang and Jiangtian Li
Oak Ridge Associated Universities

Deryn Chu
DEVCOM Army Research Laboratory

REPORT DOCUMENTATION PAGE

1. REPORT DATE	2. REPORT TYPE	3. DATES COVERED	
		START DATE	END DATE
March 2026	Technical Report	2/1/2024	2/28/2026

4. TITLE AND SUBTITLE
Additive Manufacturing of Gd-Doped CeO_2 Architectures via a Custom-Developed Printable Ceramic Resin for Ethanol Catalytic Partial Oxidation

5a. CONTRACT NUMBER	5b. GRANT NUMBER	5c. PROGRAM ELEMENT NUMBER
5d. PROJECT NUMBER	5e. TASK NUMBER	5f. WORK UNIT NUMBER

6. AUTHOR(S)
Gene Yang, Jiangtian Li, and Deryn Chu

7. PERFORMING ORGANIZATION NAME(S) AND ADDRESS(ES)
DEVCOM Army Research Laboratory
ATTN: FCDD-RLA-GC
Adelphi, MD 2078

8. PERFORMING ORGANIZATION REPORT NUMBER
ARL-TR-10305

9. SPONSORING/MONITORING AGENCY NAME(S) AND ADDRESS(ES)	10. SPONSOR/MONITOR'S ACRONYM(S)	11. SPONSOR/MONITOR'S REPORT NUMBER(S)

12. DISTRIBUTION/AVAILABILITY STATEMENT
DISTRIBUTION STATEMENT A. Approved for public release: distribution unlimited.

13. SUPPLEMENTARY NOTES
ORCIDs: Gene Yang, 0009-0002-5750-8238; Deryn Chu, 0009-0009-9051-0293

14. ABSTRACT
The development of compact and durable hydrogen generation systems for field-operable applications requires catalyst designs that integrate high activity, structural robustness, and resistance to carbon deposition. Here, we demonstrate that hydrogen production performance in ethanol catalytic partial oxidation is governed not only by catalyst chemistry, but also by how that chemistry is implemented within a reactor-relevant 3D architecture. A custom, printable gadolinium (Gd)-doped CeO_2 (GDC) ceramic resin was developed to enable stereolithography-based additive manufacturing of oxygen-vacancy-rich ceramic architectures. Using a consistent Ni–Ru–GDC catalyst system, architectural effects were systematically evaluated by comparing powder catalysts, dip-coated commercial ceramic honeycombs, and additively manufactured GDC architectures. While powder catalysts and dip-coated Al_2O_3 honeycombs exhibited comparable hydrogen production rates, the 3D-printed GDC honeycomb architecture delivered substantially enhanced hydrogen productivity. This performance improvement is attributed to the integration of redox-active, oxygen-vacancy-rich GDC as an architectural material, enabling uniform distribution of catalytic functionality throughout the macroscopic structure. Overall, this work establishes a practical, vendor-independent pathway for translating proven catalyst chemistries into structured, field-deployable reforming components and highlights the importance of architecture-aware catalyst design enabled by additive manufacturing.

15. SUBJECT TERMS
Additive Manufacturing, Gadolinium, Gd-Doped Ceria, Structured Catalysts, Catalytic Partial Oxidation, Ethanol CPOX, Hydrogen Production, Energy Sciences

16. SECURITY CLASSIFICATION OF:			17. LIMITATION OF ABSTRACT	18. NUMBER OF PAGES
a. REPORT	b. ABSTRACT	C. THIS PAGE		
UNCLASSIFIED	UNCLASSIFIED	UNCLASSIFIED	UU	24

19a. NAME OF RESPONSIBLE PERSON	19b. PHONE NUMBER *(Include area code)*
Gene Yang	(520) 691-5579

STANDARD FORM 298 (REV. 5/2020)
Prescribed by ANSI Std. Z39.18

Contents

List of Figures

List of Tables

1. Introduction

The increasing need for robust and deployable hydrogen generation technologies has driven renewed interest in reforming-based energy systems suitable for defense and field-operable applications.[1–4] In this context, the development of catalysts that combine high activity with long-term durability is essential for enabling reliable hydrogen production from liquid fuels. Ethanol is particularly attractive as a hydrogen feedstock because of its high hydrogen density, widespread availability, low toxicity, and favorable storage and handling characteristics, which align well with logistics-focused and forward-deployed energy platforms.[5–8] Among available reforming strategies, catalytic partial oxidation (CPOX) is especially advantageous due to its rapid startup capability and simplified system requirements. As an exothermic and self-sustaining process, CPOX eliminates the need for external heating or steam generation, making it well suited for compact, mobile hydrogen production units.[9–12]

Although noble-metal catalysts offer high reforming efficiency, their cost and resource limitations motivate the pursuit of alternative catalyst systems based on earth-abundant elements.[13,14] Nickel-(Ni)-based catalysts are widely regarded as practical candidates for ethanol reforming owing to their low cost, scalability, and strong activity for C–C and C–H bond activation.[15–17] Nevertheless, under high-temperature and carbon-intensive reforming conditions, Ni catalysts are susceptible to performance degradation caused by carbon accumulation and particle sintering, which ultimately compromise operational stability.[18] To overcome these limitations, ceria-based supports have been extensively investigated due to their ability to facilitate redox-driven surface regeneration. The reversible Ce^{4+}/Ce^{3+} redox couple provides oxygen storage and enhanced surface oxygen mobility, both of which play key roles in suppressing coke formation.[19–21] Further enhancement can be achieved through aliovalent doping of cerium(IV) oxide (CeO_2). In particular, substitution with gadolinium (Gd) introduces oxygen vacancies that promote faster oxygen transport and lower redox activation barriers, resulting in Gd-doped CeO_2 (GDC) supports that enable improved catalyst stability during ethanol reforming.[22]

Beyond support material design, bimetallic catalyst strategies have proven effective in further improving reforming stability.[23–29] Previously, we demonstrated that incorporating ruthenium (Ru) as a secondary metal into Ni-based catalysts supported on oxygen-vacancy-rich GDC significantly enhances catalytic durability.[30] The synergistic interaction between Ni and Ru promotes catalyst reducibility and reforming activity, while the high oxygen mobility of the GDC support material facilitates continuous oxidation of carbonaceous intermediates,

thereby suppressing coke formation. While these synergistic effects have been demonstrated using powder catalysts and dip-coated commercial ceramic honeycomb architectures, they have not been systematically examined within engineered catalyst architectures where material composition and 3D geometry can be independently controlled. Building on this previously established Ni–Ru–GDC synergy hypothesis at the support material level, the present work extends the investigation to reactor-relevant ceramic architectures to elucidate the coupled roles of catalyst chemistry and architecture in ethanol CPOX performance.

Additive manufacturing, particularly 3D printing, provides a compelling route to engineer catalyst architectures with controlled geometry and high design flexibility. Unlike conventional forming routes that rely on fixed templates or vendor-defined formats, 3D printing enables deliberate tuning of pore topology, channel connectivity, and feature size to influence mass transport, heat transfer, and effective catalyst utilization.[31–34] Such capabilities are especially attractive for reforming systems, where performance and durability are often limited not only by catalyst chemistry but also by reactor-relevant architecture constraints. Recent studies have further highlighted the ability of 3D-printed architectures to increase accessible surface area and to enable precisely defined geometries when combined with complementary materials processing methods.[35–37] These advances suggest that engineered 3D architectures can serve as a practical platform for integrating active reforming catalysts with oxide support materials that provide additional chemical functionality, such as oxygen storage and redox-driven surface regeneration. In particular, incorporating oxygen-vacancy-rich materials (e.g., GDC) into 3D-printed ceramic architectures offers a pathway to simultaneously address transport limitations and coke-related deactivation during ethanol reforming.

Accordingly, the objective of this project is to develop and evaluate additively manufactured ceramic architectures for ethanol CPOX by fabricating reactor-relevant geometries using custom-developed GDC ceramic resins, while maintaining a consistent Ni–Ru–GDC catalyst chemistry introduced via dip-coating. Rather than modifying catalyst composition, this work focuses on implementing an established Ni–Ru–GDC system within engineered 3D architectures to examine how structural realization influences reforming performance under reactor-relevant operating conditions. The significance of this approach lies in establishing a fabrication capability that enables direct integration of oxygen-vacancy-rich GDC into well-defined ceramic architectures. By extending GDC from a powder-level support material to an architectural material that defines the macroscopic catalyst structure, this study enables systematic evaluation of how architectural implementation impacts hydrogen productivity,

carbon resistance, and pore accessibility during ethanol CPOX. Collectively, this framework provides a practical pathway for translating proven catalyst chemistries into deployable, structured components suitable for compact and field-operable reforming systems.

2. Materials and Methods

Custom ceramic resins were developed for stereolithography (SLA) printing by dispersing GDC (20% Gd, fuel cell materials) powder into a photopolymerizable resin system. The base resin consisted of polyethylene glycol diacrylate (Sigma-Aldrich) as the monomer, phenylbis(2,4,6-trimethylbenzoyl)phosphine oxide (Sigma-Aldrich) as the photo initiator, and W-969 (BYK) as a dispersant. The resin–ceramic mixture was homogenized using magnetic stirring at controlled speeds to ensure uniform dispersion of the ceramic powder within the resin matrix. A key challenge during resin formulation was optimizing the ceramic powder loading to balance printability and final ceramic content. Increasing the ceramic fraction is desirable for enhancing the structural and functional properties of the sintered catalyst architectures; however, excessive ceramic loading can adversely affect SLA printability, leading to issues such as poor resin flow, incomplete curing, or feature distortion. Through iterative formulation and printing trials, an optimal balance between printability and ceramic content was established. Based on this optimization, a ceramic load of 40 wt% GDC was identified as the most suitable composition, providing reliable printing performance while maintaining structural integrity after debinding and sintering. For comparison, a commercially available alumina resin compatible with Formlabs SLA printers was used to fabricate alumina gyroid architectures.

Computer-aided design models of honeycomb and gyroid architectures were created using SolidWorks and exported as STL files for slicing. Printing was performed using an SLA printer (Form 4, Formlabs), with layer thickness set to 50 µm. Early layer exposure parameters, including laser energy density and exposure height, were optimized to ensure robust adhesion between the build platform and the initial printed layers. Additionally, exposure conditions for subsequent layers were adjusted to promote strong interlayer bonding while maintaining adequate green-state strength and stiffness. After printing, debinding schedules were designed based on thermogravimetric analysis (TGA) to minimize cracking and distortion during polymer removal. GDC samples were sintered at 1100 °C, yielding crack-free ceramic structures with uniform shrinkage.

Ni–Ru–GDC catalysts were synthesized via a wet impregnation method using $Ni(NO_3)_2 \cdot 6H_2O$ (Alfa Aesar), $RuCl_3 \cdot 3H_2O$ (Johnson Matthey), and GDC powder

as precursors.[38–40] The total metal loading was fixed at 20 wt%, with Ni and Ru incorporated at a fixed weight ratio of 9:1, while the remaining 80 wt% consisted of the oxide support (GDC). These target loadings were calculated based on precursor molecular weights, and the impregnated mass ratio was maintained identically across all samples to enable direct comparison. The required amounts of metal salts were dissolved in a 1:1 mixture of ethanol and deionized water, followed by the addition of support powders into the solution. The mixture was stirred and heated at 60 °C until a gel-like consistency was achieved, then dried at 80 °C in a convection oven. The resulting solids were calcined at 450 °C for 3 h to obtain the catalyst powders. For the preparation of dip-coated catalysts, 3D-printed architectures were immersed in a slurry composed of catalyst powder, deionized water, and polyvinylpyrrolidone in a 1:1 ratio using a dip coater (PTL-MM01). A single dip-coating cycle was employed for all samples to ensure consistency. The coated architectures were dried at 80 °C for 3 h and calcined at 450 °C for 3 h.

Catalytic activity tests were conducted in a continuous-flow fixed-bed quartz tubular reactor placed in a tube furnace and operated at 600 °C at a heating rate of 5 °C min^{-1}. Prior to reaction, the catalysts were pre-reduced under 5% H_2/N_2 flow (100 sccm) at 600 °C for 40 min. After the reduction step, the reaction was directly initiated at 600 °C without intermediate cooling. Ethanol was supplied using a syringe pump, vaporized prior to mixing with air controlled by mass flow controller. The ethanol and air feed rates were controlled to obtain an oxygen-to-carbon ratio of 1.6, selected to ensure stable H_2 production and minimized formation of CH_4 and C_2 hydrocarbons. Outlet gas flow was monitored using a mass flow meter to ensure total flow stability throughout the reaction. Reaction products were analyzed using a gas chromatograph (INFICON Micro GC), with calibration performed using certified gas standards (H_2, CO, CO_2, CH_4, C_2H_4, and C_2H_6). After each experiment, the system was cooled under N_2 (100 sccm) at a controlled rate of 10 °C min^{-1} before sample removal. To ensure data reliability, each catalytic test was conducted until steady-state operation was achieved after an initial stabilization period. Specific hydrogen production rates were averaged over the steady-state region.

3. Results and Discussion

The structural fidelity of additively manufactured ceramic architectures is critically influenced by the pre-sintering process, during which polymer removal and initial ceramic consolidation occur. The pre-sintering behavior of the printed GDC architectures was therefore examined to establish a reliable foundation for subsequent sintering and catalytic evaluation. To address this, a detailed pre-sintering baking process was developed based on TGA performed in air at a heating

rate of 1 °C min^{-1} on 3D-printed GDC samples to monitor weight loss as a function of temperature, providing critical insight into solvent evaporation, polymer decomposition, and binder burnout processes (Figure 1). The 3D-printed GDC samples exhibited distinct weight-loss events at approximately 170, 240, and 288 °C, which are consistent with staged removal of volatile species and early decomposition of organic constituents typically observed during the low-temperature debinding regime.[41]

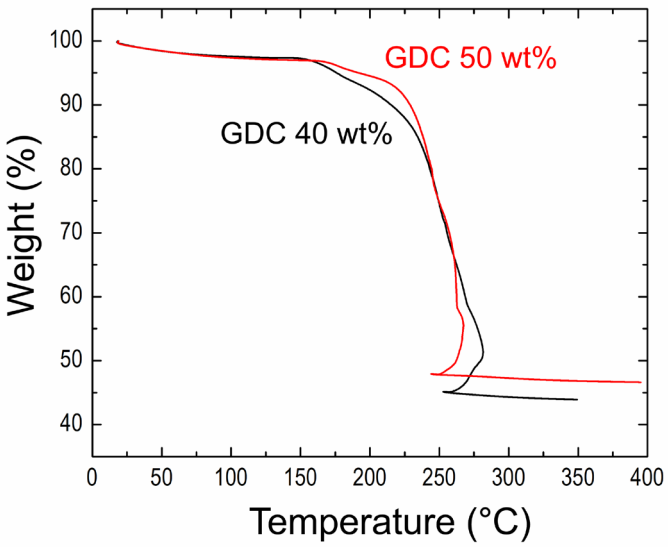

Figure 1. TGA results of 3D-printed GDC samples prepared with 40 wt% and 50 wt% resin formulations.

Based on these observations, a customized debinding schedule was designed to enable gradual removal of volatile and organic species while minimizing internal stress development within the printed architectures. This controlled thermal treatment is particularly important for complex, open-channel structures, where rapid gas evolution or uneven binder removal can lead to cracking, delamination, or distortion between printed layers.[42,43] Table 1 summarizes the optimized debinding schedule employed for the 3D-printed GDC samples. Architectures subjected to this tailored debinding process consistently exhibited crack-free morphologies, in contrast to samples processed without controlled temperature staging, which showed visible cracking and structural defects (Figure 2). Following debinding, sintering was performed at 1100 °C, resulting in dense ceramic architectures that preserved their designed geometry. The sintered GDC structures exhibited a uniform linear shrinkage of approximately 36.6% (Figure 3), indicating homogeneous ceramic consolidation throughout the architecture. Importantly, the absence of localized deformation or feature collapse confirms that the combined resin formulation, printing, and thermal processing strategy successfully translated

the designed 3D geometry into a mechanically robust ceramic structure suitable for subsequent catalytic evaluation.

Table 1. Debinding schedule details for the 3D-printed GDC samples.

Time step (min)	End temp (°C)	Rate (°C/min)
0	20	. . .
60	50	0.5
120	50	0
500	100	0.1
120	100	0
300	130	0.1
360	130	0
200	150	0.1
240	150	0
250	175	0.1
240	175	0
350	210	0.1
360	210	0
500	260	0.1
360	260	0
400	300	0.1
360	300	0
1000	400	0.1
120	400	0
380	20	1

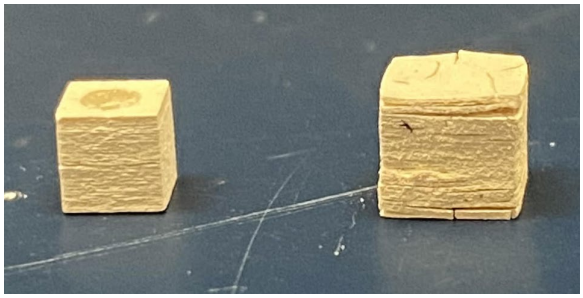

Figure 2. Images of 3D-printed GDC samples after debinding. The sample processed using the optimized, temperature-controlled debinding schedule (left) substantially reduced cracking and minimal layer distortion, whereas the sample processed without staged temperature control (right) shows pronounced cracking and interlayer deformation.

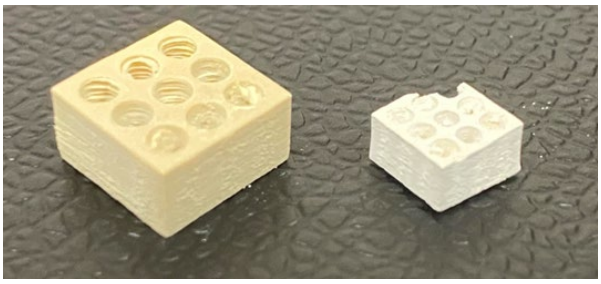

Figure 3. Images of 3D-printed GDC samples showing the green body before thermal processing (left) and the fully sintered ceramic after debinding and sintering (right). The sintered sample retains the designed honeycomb geometry with uniform shrinkage.

With the structural integrity of the additively manufactured architectures established, the catalytic performance of the Ni–Ru–GDC system was evaluated under ethanol CPOX conditions and compared across different structural implementations (Figure 4). The specific hydrogen production rate of the Ni–Ru–GDC powder catalyst was measured to be approximately 2.46-mol H_2 g^{-1} h^{-1}. A comparable value (2.44-mol H_2 g^{-1} h^{-1}) was obtained when the same catalyst chemistry was implemented via dip-coating onto a commercial Al_2O_3 honeycomb, indicating that simple integration of the catalyst on an inert ceramic substrate does not inherently enhance hydrogen productivity. To examine the effect of 3D architectural design independent of support chemistry, an Al_2O_3 gyroid structure was selected as a representative 3D-printed architecture. Gyroid geometry is a triply periodic minimal surface characterized by continuous curvature, high surface-area-to-volume ratio, and fully interconnected pore networks, which are advantageous for promoting uniform gas distribution, minimizing transport dead zones, and enhancing effective catalyst utilization.[44–46] Consistent with these attributes, the Al_2O_3 gyroid architecture exhibited a markedly increased hydrogen production rate of approximately 4.86-mol H_2 g^{-1} h^{-1}, nearly doubling the performance relative to both the powder catalyst and the dip-coated commercial honeycomb. This improvement underscores the critical role of architecture in governing mass transport and accessibility of active sites during ethanol reforming.

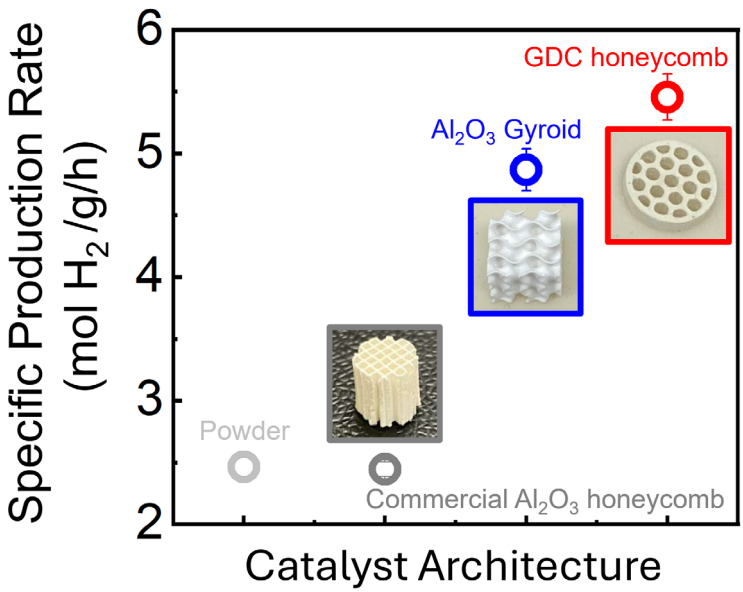

Figure 4. Specific hydrogen production rates of the Ni–Ru–GDC catalyst system implemented in different architectural configurations during ethanol CPOX at 600 °C.

While the gyroid architecture could also be successfully printed using the custom GDC resin (Figure 5), optimization of the debinding process for this more complex geometry remains ongoing. Therefore, to reliably evaluate the influence of incorporating oxygen-vacancy-rich GDC as an architectural material, a simpler and more robust honeycomb geometry was employed for the GDC-based structures. The 3D-printed GDC architectures were fabricated in a honeycomb configuration with a porosity of 30 ppi (hexagon size: 0.9 mm), a diameter of 7.25 cm, and a thickness of 1.7 mm after debinding and sintering (Figure 6). This geometry provided mechanically stable, open-channel structures with well-defined flow paths, enabling reproducible catalytic testing.

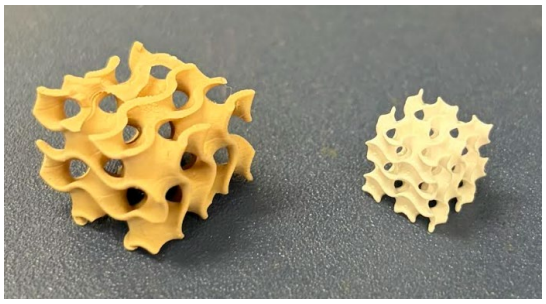

Figure 5. Comparison of additively manufactured gyroid architectures fabricated using GDC (left) and Al_2O_3 (right) ceramic resins, demonstrating comparable geometric fidelity and structural resolution.

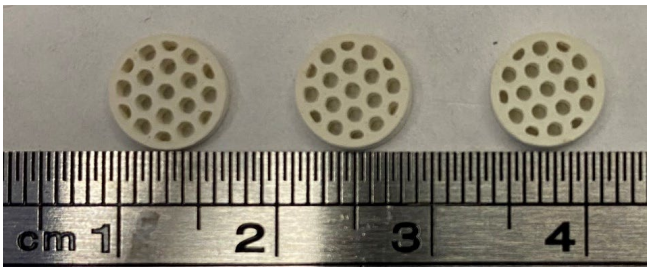

Figure 6. 3D-printed GDC honeycomb architectures after debinding and sintering, illustrating uniform geometry retention and reproducible fabrication.

Among all tested configurations, the 3D-printed GDC honeycomb architecture exhibited the highest hydrogen production rate of 5.46-mol H_2 g^{-1} h^{-1}. Because the active metal composition was kept constant across all samples, this additional performance gain is attributed to the combined effects of architectural implementation and support-material chemistry. By extending GDC from a powder-level support to an architectural material that defines the macroscopic catalyst structure, the redox-active and oxygen-vacancy-rich nature of GDC is distributed throughout the reactor-relevant architecture, facilitating enhanced oxygen mobility, improved removal of carbonaceous intermediates, and sustained access to active sites during reforming.[47–49] This interpretation is further supported by post-reaction visual examination of the tested structures, which revealed that the GDC honeycomb exhibited the least apparent carbon deposition among all evaluated configurations. In contrast to the Al_2O_3-based architectures, the GDC honeycomb retained clean and open channels after reaction, with minimal darkening or pore blockage, indicating effective suppression of carbon accumulation under ethanol CPOX conditions (Figure 7). Overall, these results demonstrate that hydrogen productivity during ethanol CPOX is governed not only by catalyst chemistry but also by how that chemistry is implemented within a 3D architecture. In particular, the combination of a structurally robust honeycomb geometry with an oxygen-vacancy-rich GDC framework enables synergistic enhancement of reforming performance beyond what is achievable using powder catalysts or dip-coated commercial supports.

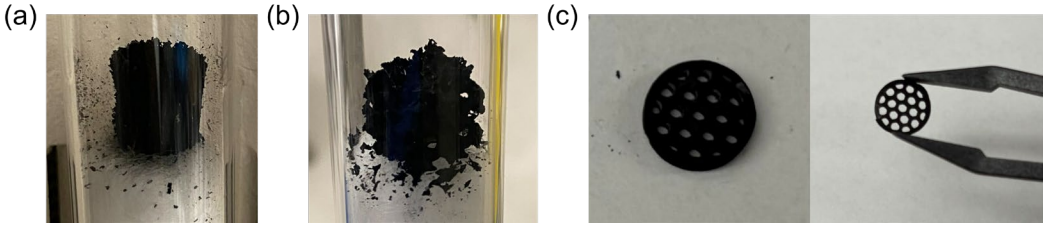

Figure 7. Representative images of structured catalysts after ethanol CPOX testing. (a) Commercial Al_2O_3 honeycomb and (b) Al_2O_3 gyroid exhibit pronounced darkening and visible accumulation of dark fragments after reaction, whereas (c) the 3D-printed GDC honeycomb retains an open-channel morphology with minimal visible blockage.

4. Future Perspective

Commercially available catalyst architectures, such as alumina honeycombs, offer well-established performance but inherently require reliance on external vendors. This dependence imposes significant constraints on material selection, geometry, size, and quantity, often accompanied by long lead times and minimum order requirements. Such limitations become particularly restrictive when non-standard designs, rapid iteration, or mission-specific configurations are needed. In contrast, the present work demonstrates that catalyst architectures can be fabricated in-house using custom-developed ceramic resins and additive manufacturing. By decoupling catalyst architecture fabrication from commercial supply chains, both the material composition and 3D architecture can be tailored on demand. This approach enables rapid adjustment of geometry, size, and production volume without tooling changes or vendor negotiation, providing a level of flexibility that is not achievable with conventional commercial architectures. While initial development of printable ceramic resins and process optimization requires upfront effort, once established, this platform allows for significantly reduced fabrication lead times for customized components and lowers the cost barrier for small-batch or prototype production. More importantly, the ability to rapidly design, fabricate, and test catalyst structures accelerates experimental iteration and technology maturation. From an Army perspective, this capability offers a strategic advantage by enabling mission-adaptable catalyst architectures, reduced reliance on external suppliers, and on-demand fabrication under constrained or rapidly changing operational requirements. Such flexibility is particularly relevant for expeditionary energy systems, forward-deployed fuel processing units, and distributed hydrogen generation, where logistics, supply resilience, and adaptability are critical. The demonstrated 3D-printing framework therefore provides a pathway toward scalable, resilient, and customizable catalyst systems aligned with Army operational needs.

5. Conclusion

This study demonstrates that hydrogen production performance in ethanol CPOX is governed not only by catalyst chemistry, but also by how that chemistry is implemented within a reactor-relevant 3D architecture. In addition to establishing the performance benefits of architectural design, this work demonstrates the successful development of a custom, printable GDC ceramic resin, enabling additive manufacturing of oxygen-vacancy-rich ceramic architectures using SLA. Using a consistent Ni–Ru–GDC catalyst system, the effects of architectural implementation were systematically evaluated through comparison of powder catalysts, dip-coated commercial ceramic honeycombs, and additively

manufactured architectures. While the powder catalyst and dip-coated Al_2O_3 honeycomb exhibited comparable hydrogen production rates, substantial performance enhancement was achieved through 3D structuring. The Al_2O_3 gyroid architecture confirmed that architectural design alone can significantly improve hydrogen productivity by enhancing gas transport and effective catalyst utilization. Further improvement was achieved when GDC was employed as an architectural material, with the 3D-printed GDC honeycomb delivering the highest hydrogen production rate and exhibiting the least apparent carbon deposit after reaction. Collectively, these results establish that extending GDC from a powder-level support to a printable architectural framework enables uniform distribution of redox functionality and oxygen mobility throughout the catalyst structure, leading to enhanced hydrogen productivity and improved resistance to carbon accumulation. More broadly, this work highlights the importance of architecture-aware catalyst design and demonstrates a practical, vendor-independent pathway for translating proven catalyst chemistries into compact, durable, and field-operable hydrogen generation systems through additive manufacturing.

6. References

1. Dou B, Song Y, Wang C, Chen H, Xu Y. Hydrogen production from catalytic steam reforming of biodiesel byproduct glycerol: issues and challenges. Renew Sustain Energy Rev. 2014;30:950–960. https://doi.org/10.1016/j.rser.2013.11.029

2. Mattos LV, Jacobs G, Davis BH, Noronha FB. Production of hydrogen from ethanol: review of reaction mechanism and catalyst deactivation. Chem Rev. 2012;112(7):4094–4123. https://doi.org/10.1021/cr2000114

3. Iulianelli A, Ribeirinha P, Mendes A, Basile A. Methanol steam reforming for hydrogen generation via conventional and membrane reactors: a review. Renew Sustain Energy Rev. 2014;29:355–368. https://doi.org/10.1016/j.rser.2013.08.032

4. Soboń A, Słyś D, Ruszel M, Wiącek A. Prospects for the use of hydrogen in the Armed Forces. Energies. 2021;14(21):7089. https://doi.org/10.3390/en14217089

5. Chaubey R, Sahu S, James OO, Maity S. A review on development of industrial processes and emerging techniques for production of hydrogen from renewable and sustainable sources. Renew Sustain Energy Rev. 2013;23:443–462. https://doi.org/10.1016/j.rser.2013.02.019

6. Zanchet D, Santos JBO, Damyanova S, Gallo JMR, Bueno JMC. Toward understanding metal-catalyzed ethanol reforming. ACS Catal. 2015;5(6):3841–3863. https://doi.org/10.1021/cs5020755

7. Ni M, Leung DYC, Leung MKH. A review on reforming bio-ethanol for hydrogen production. Int J Hydrogen Energy. 2007;32(15):3238–3247. https://doi.org/10.1016/j.ijhydene.2007.04.038

8. Augusto BL, Costa LOO, Noronha FB, Colman RC, Mattos LV. Ethanol reforming over Ni/CeGd catalysts with low Ni content. Int J Hydrog Energy. 2012;37(17):12258–12270. https://doi.org/10.1016/j.ijhydene.2012.05.127

9. Ma R, Xu B, Zhang X. Catalytic partial oxidation (CPOX) of natural gas and renewable hydrocarbons/oxygenated hydrocarbons—a review. Catal Today. 2019;338:18–30. https://doi.org/10.1016/j.cattod.2019.06.025

10. Hohn KL, Lin Y-C. Catalytic partial oxidation of methanol and ethanol for hydrogen generation. ChemSusChem. 2009;2(10):927–940. https://doi.org/10.1002/cssc.200900104

11. Jung H et al. Fast start-up reactor for partial oxidation of methane with electrically-heated metallic monolith catalyst. J Power Sources. 2003;124(1): 76–80. https://doi.org/10.1016/S0378-7753(03)00604-9

12. Chen W-H et al. A critical and systematic review of sustainable hydrogen production from ethanol/bioethanol: steam reforming, partial oxidation, and autothermal reforming. Fuel. 2023;333(2):126526. https://doi.org/10.1016/j.fuel.2022.126526

13. Rosha P, Ali FM, Ibrahim H. Recent advances in hydrogen production through catalytic steam reforming of ethanol: advances in catalytic design. Can J Chem Eng. 2023;101(10):5498–5518. https://doi.org/10.1002/cjce.24859

14. Ogo S, Sekine Y. Recent progress in ethanol steam reforming using non-noble transition metal catalysts: a review. Fuel Process Technol. 2020;199:106238. https://doi.org/10.1016/j.fuproc.2019.106238

15. Xu W et al. Steam reforming of ethanol on Ni/CeO_2: reaction pathway and interaction between Ni and the CeO_2 support. ACS Catal. 2013;3(5):975–984. https://doi.org/10.1021/cs4000969

16. Liu Z et al. Ambient pressure XPS and IRRAS investigation of ethanol steam reforming on Ni–CeO_2(111) catalysts: an *in situ* study of C–C and O–H bond scission. Phys Chem Chem Phys. 2016;18:16621–16628. https://doi.org/10.1039/C6CP01212D

17. Fatsikostas AN, Verykios XE. Reaction network of steam reforming of ethanol over Ni-based catalysts. J Catal. 2004;225(2):439–452. https://doi.org/10.1016/j.jcat.2004.04.034

18. Karim AM et al. A comparative study between Co and Rh for steam reforming of ethanol. Appl Catal B Env. 2010;96(3–4):441–448. https://doi.org/10.1016/j.apcatb.2010.02.041

19. Gupta A, Waghmare UV, Hegde MS. Correlation of oxygen storage capacity and structural distortion in transition-metal-, noble-metal-, and rare-earth-ion-substituted CeO_2 from first principles calculation. Chem Mater. 2010;22(18):5184–5198. https://doi.org/10.1021/cm101145d

20. Kehoe AB, Scanlon DO, Watson GW. Role of lattice distortions in the oxygen storage capacity of divalently doped CeO_2. Chem Mater. 2011;23(20):4464–4468. https://doi.org/10.1021/cm201617d

21. Silva AGM et al. $Ce_{1-x}Sm_xO_{1.9-\delta}$ nanoparticles obtained by microwave-assisted processing: an efficient application for catalytic oxidation of α-bisabolol. Catal Sci Technol. 2014;4:814–821. https://doi.org/10.1039/C3CY00788J

22. Tojira O, Lomonaco JG, Sesuk T, Charojrochkul S, Tepamatr P. Enhancement of hydrogen production using Ni catalysts supported by Gd-doped ceria. Heliyon. 2021;7(10):e08202. https://doi.org/10.1016/j.heliyon.2021.e08202

23. Hong DQT, Do BL, Ha CA, Nguyen T, Loc LC. Role of ruthenium in modified $CeNi_{1-x}Ru_xO_3$ perovskite catalysts for the bireforming of methane. Energy Fuels. 2025;39(2):1341–1361. https://doi.org/10.1021/acs.energyfuels.4c04915

24. Carbajal-Ramos IA et al. Catalytic behavior of Ru supported on $Ce_{0.8}Zr_{0.2}O_2$ for hydrogen production. Appl Catal B Env. 2016;181:58–70. https://doi.org/10.1016/j.apcatb.2015.07.025

25. Hung CC, Chen SL, Liao Y, Chen CH, Wang J. Oxidative steam reforming of ethanol for hydrogen production on M/Al_2O_3. Int J Hydrog Energy. 2012;37:4955–4966. https://doi.org/10.1016/J.IJHYDENE.2011.12.060

26. Liguras DK, Kondarides DI, Verykios XE. Production of hydrogen for fuel cells by steam reforming of ethanol over supported noble metal catalysts. Appl Catal B Env. 2003;43(4):345–354. https://doi.org/10.1016/S0926-3373(02)00327-2

27. Chiu W-C, Horng R-F, Chou H-M. Hydrogen production from an ethanol reformer with energy saving approaches over various catalysts. Int J Hydrog Energy. 2013;38(6):2760–2769. https://doi.org/10.1016/j.ijhydene.2012.12.068

28. Liu F et al. Synergistic effects of in-situ exsolved Ni–Ru bimetallic catalyst on high-performance and durable direct-methane solid oxide fuel cells. J Am Chem Soc. 2024;146(7):4704–4715. https://doi.org/10.1021/jacs.3c12121

29. Liu F et al. Process-intensified protonic ceramic fuel cells for power generation, chemical production, and greenhouse gas mitigation. Joule. 2023;7(6):1308–1332. https://doi.org/10.1016/j.joule.2023.05.009

30. Yang G, Li J, Chu D. Synergistic effect of bimetallic Ni–Ru and oxygen-vacancy-rich Gd-doped CeO_2 for enhanced hydrogen production and coke-resistant stability in ethanol partial oxidation. Int J Hydrog Energy. 2026;217:153949. https://doi.org/10.1016/j.ijhydene.2026.153949

31. Ferrage L, Bertrand G, Lenormand P, Grossin D, Ben-Nissan B. A review of the additive manufacturing (3DP) of bioceramics: alumina, zirconia (PSZ) and hydroxyapatite. J Aust Ceram Soc. 2017;53:11–20. https://doi.org/10.1007/s41779-016-0003-9

32. Caballero JJB et al. Advanced application of a geometry-enhanced 3D-printed catalytic reformer for syngas production. Energy Convers Manag. 2023;287:117071. https://doi.org/10.1016/j.enconman.2023.117071

33. Jacquot C et al. A multi-scale study of 3D printed Co–Al_2O_3 catalyst monoliths versus spheres. Chem Eng J Adv. 2023;16:100538. https://doi.org/10.1016/j.ceja.2023.100538

34. Mastroianni L et al. DLP 3D printing of alumina catalyst architectures: design, kinetics and modeling of structure effects on catalyst performance. Chem Eng J. 2024;501:157691. https://doi.org/10.1016/j.cej.2024.157691

35. Yang G, Nam SH, Han G, Fang NX, Lee D. Achieving fast oxygen reduction on oxide electrodes by creating 3D multiscale micro-nano structures for low-temperature solid oxide fuel cells. ACS Appl Mater Interfaces. 2023;15(43):50427–50436. https://doi.org/10.1021/acsami.3c07115

36. Chen J et al. 3D printing enhanced catalysis for energy conversion and environment treatment. DeCarbon. 2023;2:100019. https://doi.org/10.1016/j.decarb.2023.100019

37. Li N et al. Revolutionizing catalytic water treatment: a critical review on the role of 3D-printed catalysts. Sep Purif Technol. 2025;363(3):132194. https://doi.org/10.1016/j.seppur.2025.132194

38. Sietsma JRA et al. Ordered mesoporous silica to study the preparation of Ni/SiO_2 ex nitrate catalysts: impregnation, drying, and thermal treatments. Chem Mater. 2008;20(9):2921–2931. https://doi.org/10.1021/cm702610h

39. Rad SJH, Haghighi M, Eslami AA, Rahmani F, Rahemi N. Sol–gel vs. impregnation preparation of MgO and CeO_2 doped Ni/Al_2O_3 nanocatalysts used in dry reforming of methane: effect of process conditions, synthesis method and support composition. Int J Hydrog Energy. 2016;41(11):5335–5350. https://doi.org/10.1016/j.ijhydene.2016.02.002

40. Chouillet C, Villain F, Kermarec M, Lauron-Pernot H, Louis C. Relevance of the drying step in the preparation by impregnation of Zn/SiO_2 supported catalysts. J Phys Chem B. 2003;107(15):3565–3575. https://doi.org/10.1021/jp022481+

41. Wang K et al. Study of defect-free debinding green body of ceramic formed by DLP technology. Ceram Int. 2020;46(2):2438–2446. https://doi.org/10.1016/j.ceramint.2019.09.237

42. Kim J et al. Effect of non-reactive diluent on defect-free debinding process of 3D-printed ceramics. Addit Manuf. 2023;67:103475. https://doi.org/10.1016/j.addma.2023.103475

43. McAleer EG et al. Binder removal from ceramic stereolithography green bodies: a neutron imaging and thermal analysis study. J Am Ceram Soc. 2023;106(7):4399–4410. https://doi.org/10.1111/jace.19095?urlappend=%3Futm_source%3Dresearchgate.net%26utm_medium%3Darticle

44. Luo J-W et al. Macroscopic transport properties of gyroid structures based on pore-scale studies: permeability, diffusivity and thermal conductivity. Int J Heat Mass Transf. 2020;146:118837. https://doi.org/10.1016/j.ijheatmasstransfer.2019.118837

45. Reid S, Lecarpentier F, Symons D, Watson M. Can 3D-printed catalysts improve hydrogen peroxide thruster performance? An experimental and numerical study. Chem Eng Sci. 2025;302(A):120783. https://doi.org/10.1016/j.ces.2024.120783

46. Jivrakh KB et al. A 3D-printed metal-supported gyroid Ni/Al_2O_3 catalyst for CO_2 methanation. J CO_2 Util. 2025;98:103143. https://doi.org/10.1016/j.jcou.2025.103143

47. Yang Z, Fu Z, Zhang Y, Wu R. Direct CO oxidation by lattice oxygen on Zr-doped ceria surfaces. Catal Lett. 2011;141:78–82. https://doi.org/10.1007/s10562-010-0446-5

48. Ben-Arfa BAE, Abanades S, Salvado IMM, Ferreira JMF, Pullar RC. Robocasting of 3D-printed and sintered ceria scaffold structures for solar thermochemical fuel production from the splitting of CO_2. Nanoscale. 2022;14:4994–5001. https://doi.org/10.1039/D2NR00393G

49. Sas Brunser S et al. Solar-driven redox splitting of CO_2 using 3D-printed ceria structures. Adv Mater Interfaces. 2023;10(30):2300452. https://doi.org/10.1002/admi.202300452

List of Symbols, Abbreviations, and Acronyms

3D	Three-Dimensional
CeO_2	Cerium(IV) Oxide; Ceria
CPOX	Catalytic Partial Oxidation
GC	Gas Chromatograph
Gd	Gadolinium
GDC	Gd-Doped CeO_2
Ni	Nickel
Ru	Ruthenium
SLA	Stereolithography
TGA	Thermogravimetric Analysis

1 (PDF)	DEFENSE TECHNICAL INFORMATION CTR DTIC OCA
1 (PDF)	DEVCOM ARL FCDD RLB CI TECH LIB